PERGAMON

International Journal of Heat and Mass Transfer 44 (2001) 2643–2659

International Journal of HEAT and MASS TRANSFER

www.elsevier.com/locate/ijhmt

A hydrodynamic and thermodynamic simulation of droplet impacts on hot surfaces, Part II: validation and applications

Dalton J.E. Harvie, David F. Fletcher *

Department of Chemical Engineering, University of Sydney, Sydney, NSW 2006, Australia

Received 13 January 2000; received in revised form 18 September 2000

Abstract

A model was previously presented to simulate the behaviour of an axisymmetric droplet impacting on a hot solid surface in the film boiling region (D.J.E. Harvie, D.F. Fletcher, International Journal of Heat and Mass Transfer 44 (2001) 2633–2642). In this paper comparisons against experimental water and *n*-heptane droplet impacts are made which validate the hydrodynamic and thermodynamic predictive capabilities of the model. Specifically, it is shown that the hydrodynamic behaviour of impacting droplets is predicted accurately below a Weber number of approximately 30, while above this level, at least the initial hydrodynamical aspects of an impact can be predicted. The model is found to reproduce the thermodynamic behaviour of actual droplet impacts when no contact between the solid and liquid phases occurs.

Keywords: Film boiling; Droplet impacts; Volume of fluid (VOF); Leidenfrost; Spray cooling

1. Introduction

This paper forms the second part of a two-part study on film boiling droplet impacts. Part I of the series presented a model capable of simulating such impacts [1]. The model is composed of a volume of fluid (VOF) algorithm used to simulate gross droplet deformation, coupled to a one-dimensional algorithm used to simulate fluid flow within the vapour layer existing between the liquid and solid phases. The code which implements this model is called 'BOUNCE'.

The primary purpose of the present paper is to validate the BOUNCE code in simulating both saturated and subcooled film boiling droplet impacts. Subcooled impacts are defined as impacts where the initial temperature of the droplet is below the saturation temperature of the liquid, whereas saturated impacts are defined as those where the initial temperature of the liquid is the saturation temperature of the liquid. A secondary purpose of the paper is to examine the general behaviour of saturated and subcooled film boiling impacts, especially with reference to the conditions existing within the viscous vapour layer during these complex multi-phase interactions. Note that the nature of subcooled and saturated film boiling impacts is quite different – subcooled film boiling impacts are characterised by significantly higher heat transfer rates than their saturated counterparts.

The study by Wachters and Westerling [2] was one of the first experimental investigations into the dynamics and heat transfer during saturated film boiling droplet impacts. In these experiments water droplets, having an initial diameter of 2.3 mm, impacted on a polished gold surface whose initial temperature was varied between 200°C and 400°C. Wachters and Westerling used a series of high-speed photographs to record droplet impact dynamics, and a heat loss analysis from the solid impact material to measure the heat transfer characteristics of the impacts.

Wachters and Westerling identified three different dynamical regimes of droplet impact, defined in terms of the non-dimensional Weber number,

$$We = \frac{\rho d v^2}{\sigma}.$$

* Corresponding author. Tel.: +61-2-9351-4147; fax: +61-2-9351-2854.

E-mail address: davidf@chem.eng.usyd.edu.au (D.F. Fletcher).

0017-9310/01/$ - see front matter
PII: S0017-9310(00)00304-5

Nomenclature

d	droplet diameter (m)
e	energy (J)
F	volume of fluid (VOF) function
Kn	Knudsen number
r_{av}	radius for averaging (m)
R_a	surface roughness (m)
T	temperature (K)
v	normal droplet impact velocity (m/s)
We	Weber number
y_a	air volume fraction

Greek symbols

ρ	droplet density (kg/m^3)
σ	surface tension (N/m)

Subscripts

i	initial
l	liquid
ll	liquid side of liquid–vapour interface
lv	vapour side of liquid–vapour interface
s	solid
ss	solid side of solid–vapour interface
sv	vapour side of solid–vapour interface
v	vapour

At Weber numbers of less than 30, droplets impact and expand over the surface, before recollecting and rebounding as one discrete mass of fluid. For Weber numbers between 30 and 80, droplets impact and expand over the surface as the lower velocity droplets do, but during the recollection and rebound stage, separate into a number of smaller, or satellite, droplets. When droplets impact the solid with a Weber number greater than 80, droplet disintegration is observed during the initial expansion phase, and often only a small percentage of the initial droplet volume recollects after the impact into one major fluid body.

Wachters and Westerling also showed in their experiments that film boiling impacts only occurred above an initial solid temperature of 370°C, which is considerably higher than the minimum steady-state film boiling temperature for water, reported to be around 250°C [3,4]. Also, the proportion of droplet liquid vaporised during the impacts was always less than 1% of the total droplet volume.

Another study to consider saturated film boiling impacts was that by Groendes and Mesler [5]. In this study, droplets having a large initial diameter of 4.7 mm were impacted on a quartz surface whose initial temperature was 462°C. The dynamics of droplet impingement were recorded using a series of high-speed photographs, and the surface temperature of the solid during the impact was measured using a platinum film resistance thermometer.

The Groendes and Mesler experiments showed that even with a low thermal diffusivity material such as quartz, the temperature drop of the solid surface during a droplet impact was only small, of the order of 20°C. It was also shown that the temperature of the surface during each impact was highly oscillatory, suggesting that the height of vapour layer during an impact is also oscillatory.

There are a far greater number of subcooled experimental impact studies available than saturated impact studies, however, few authors have appreciated the dependence droplet subcooling has on impact behaviour. Indeed, in most studies the initial temperature of the liquid is not varied, and in some cases not even specified.

The experimental study by Inada et al. [6] was one of the first to perform subcooled droplet impacts where the degree of droplet subcooling was varied. In their study, water droplets, having an initial diameter of 4 mm, impacted on a polished copper surface, whose surface temperature was measured using a series of thermocouples. It was found by Inada et al., that in the nucleate, transition and film boiling regimes, a change in initial droplet subcooling from 2°C to 88°C could increase the heat transfer during an impact by over an order of magnitude, and could also significantly change the droplet impact dynamical behaviour.

The study performed by Qiao and Chandra [7] is notable because while the initial liquid temperature was held constant in these experiments, the tests were performed using both water and *n*-heptane, and the initial temperature of the stainless steel impact surface was varied between 150°C and 320°C. An excellent series of photographs was produced to record the droplet impact dynamics, and the surface temperature of the impact material was measured using a fine gauge thermocouple. Some of these tests were performed in a low gravity environment.

Qiao and Chandra have found that while transition, or perhaps film boiling impacts occurred with *n*-heptane above an initial solid temperature of approximately 200°C, similar impacts could not be replicated with water, even when the initial temperature of the solid was raised to the limit of the experimental equipment, namely 320°C. This phenomenon was explained to be a result of the different surface tension values between the two liquids, which affects the ability of liquids to nucleate at the solid interface. A similar series of experiments, performed with only *n*-heptane, was conducted by Chandra and Avedisian [8].

The experimental study by Chen and Hsu [9] was motivated by the need to determine local heat transfer rates during different boiling regimes. In this study, subcooled water droplets impacted a low thermal diffu-

sivity Inconel surface, whose initial temperature ranged between 150°C and 550°C. Impact surface temperatures were measured using a fine gauge surface mounted thermocouple, and local heat transfer rates were calculated by the authors from these measurements. It was found by Chen and Hsu [9] that heat transfer rates under impacting subcooled droplets varied from approximately 1×10^6 W/m^2 during low temperature single phase heat transfer impacts up to approximately 2×10^7 W/m^2 during nucleate boiling impacts with an initial solid temperature of 500°C.

The study by Inada et al. [10] is unique in that the authors were able to measure vapour layer thicknesses beneath impinging water droplets. Using an expanded laser beam, the resolution of their experimental technique allowed vapour layer heights greater than 2 μm to be measured. Water droplets, having an initial diameter of 2.3 mm and an impact Weber number within the range 12–15, were impacted on a polished copper surface whose initial temperature was varied between 180°C and 500°C. Droplets having initial subcoolings of either 2°C or 88°C were used.

Inada et al. [10] have found that with the 88°C subcooled droplets, no vapour layer was detectable in the initial period of impact, irrespective of the initial solid temperature employed. However, a vapour layer of height less than 5 μm was detected in the latter half of the subcooled impacts when the initial solid temperature was set above 420°C. They also found that for the nearly saturated droplets, when the initial surface temperature was above 220°C, a vapour layer was almost always apparent, and that the height of this vapour layer was generally larger and more oscillatory than the layers under the subcooled droplets.

Other experimental subcooled droplet impact studies have been performed by McGinnis and Holman [11], Holman et al. [12], Pedersen [13], Seki et al. [14], Makino and Michiyoshi [15], Xiong and Yuen [16] and Bernardin et al. [17] amongst others.

Validation of the BOUNCE model is accomplished in this paper by comparing documented experimental impacts, namely those presented in the Wachters and Westerling [2], Groendes and Mesler [5] and Qiao and Chandra [7] studies discussed above, against simulations of the same impacts. This is accomplished first for saturated impacts, followed by subcooled impacts.

2. Saturated film boiling droplet impacts

In this section, three individual saturated droplet impacts are used to validate the BOUNCE code. The first two impacts are used to validate the hydrodynamic ability of BOUNCE in simulating a saturated impact, while the third impact examines the thermodynamic ability of BOUNCE in simulating a saturated impact.

2.1. The Wachters and Westerling $We = 15$ impact

Fig. 1(a) shows a droplet impact presented in Wachters and Westerling [2], and Fig. 1(b) shows the BOUNCE simulation of the same impact. The Weber number for this impact was 15, corresponding to an impact velocity of 0.63 m/s for the 2.3 mm diameter droplet. The initial solid surface temperature used in all the Wachters and Westerling experiments considered in this study was 400°C.

The BOUNCE simulation shown in Fig. 1(b) was performed using 50×140 square cells over a computational domain of 0–2.5 mm radially and -0.1–6.9 mm vertically. The code took approximately 13,000 iterations to simulate 18 ms of impact, giving an average computational timestep of 1.4 μs. Such a small timestep is a result of the inherently stiff nature of the physical problem.

The droplet images shown in Fig. 1(b) were generated by plotting the VOF contour line, $F = 0.5$. As the computation was performed in two-dimensional cylindrical coordinates, each contour plot was reflected around the axis of the droplet to produce the cross-sectional images displayed in the figure. The computational images were generated at times which approximately correspond to the times of the experimental images.

Comparing the simulated and experimental images of Fig. 1, it is evident that BOUNCE predicts the dynamic behaviour of the droplet well. The first four frames, that is up to 1 ms, show that upon impact, a wave of water at the bottom surface of the droplet moves radially outward from the centre. The crest of this wave is very close to the solid, but with increasing distance from the centre, moves slightly upward. Due to reflection of light off the outer surface of the photographed droplet, it is not possible to directly compare the behaviour of the droplet base within the vapour layer. However, consistent with the simulation, photographs do show that the vapour layer height is very small at the extremity of the layer.

The next five frames, from 1.5 to 3.5 ms, show the droplet spreading out over the surface. By this stage, the thickness of the vapour layer has increased to a visible level in the computational images, however, the resolution of the photographed impact does not allow validation of this behaviour.

There appears to be a distinctive central feature within the droplet shown in photograph nine (3.85 ms) of the experimental impact. It is not clear from the photograph whether this feature is a hump of fluid or a void region within the droplet. The computational image at approximately the same time shows a hump of fluid which is less pronounced than the feature shown in the experimental impact.

The last seven frames, from 5 ms onwards, show the droplet recollecting as it is pushed away from the

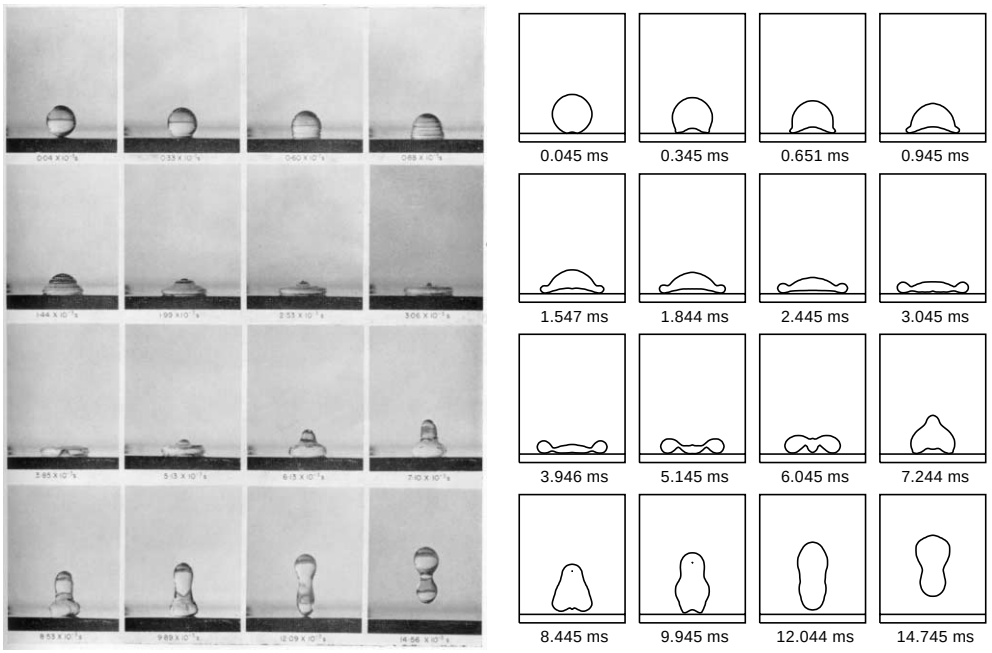

Fig. 1. The $We = 15$ impact performed by Wachters and Westerling. Frame (a) shows the experimental photographs (taken from [2]), while frame (b) shows the simulation results. The initial diameter of the droplet was 2.3 mm.

surface. During this period the vapour layer geometry and vapour layer height change quickly and substantially, but it is not possible to validate this behaviour from the photographed images of Fig. 1(a). BOUNCE predicts the droplet recoil process well, particularly the dumb-bell shape shown in the final photograph and computational frame.

A small void area, or bubble, is shown in frames 13 and 14 of the computational images. This void region was formed at approximately 6.7 ms, when a small vapour layer region at the centreline of the droplet was enclosed in the liquid. Although the resolution of the photographic images is not as high as the resolution of the computational images, bubble formation is not observed in the experimental impact during the droplet recollecting process.

Void regions within fluid volumes can be formed by VOF codes when a channel of void within a fluid region becomes narrower than the computational cell dimensions. In such instances, the discrete nature of the VOF function can act to sever the channel of void, effectively creating bubbles inside the fluid volume. Surface tension forces re-enforce this phenomenon by combining small void regions into larger void regions or bubbles. Thus, when bubbles, which have dimensions of the order of the computational cell size are formed in computations, their existence must be treated with caution. The bubble shown in Fig. 1(b) is of a similar size than the computational cell dimensions, so its presence may not be realistic.

Computations were continued past the last experimental photograph shown in Fig. 1(b) for a further 3 ms. These showed that the dumb-bell shape shown at 14.7 ms reforms into one oscillating droplet within a few milliseconds.

It should be noted that as the photographs shown in Fig. 1(a) are a record of a single droplet impact rather than an average of how many such similar droplets would behave. Thus, caution should be exercised when comparing the finer details of the two results.

Fig. 2 shows the maximum height and radius of the droplet during both the simulated and experimental impacts. The correlation between the two results is generally good, the BOUNCE model accurately predicting the oscillation period and overall behaviour of the experimental droplet.

The height of the droplet during the recollecting period is underpredicted in the simulations by approximately 1 mm. This underprediction is consistent with differences between the photographic and computational images of Fig. 1, which show that the experimental droplet generally has a smaller mid-height radius than the computational droplet during the recoil period, and consequently, a larger axial height.

The minimum height of the vapour layer during the Wachters and Westerling $We = 15$ impact was calculated

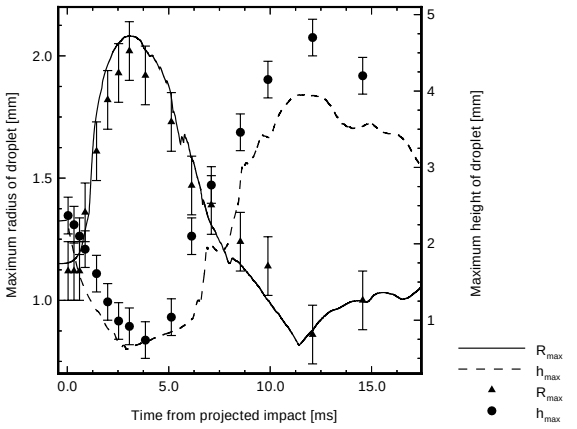

Fig. 2. The maximum droplet radius and height during the Wachters and Westerling $We = 15$ impact. Symbols indicate experimental values measured from the photographs of Fig. 1, the continuous lines the results from the BOUNCE simulation. The error-bars attached to the symbols indicate the accuracy of the experimental measurements.

by BOUNCE as approximately 3 μm, however, the minimum height averaged over the duration of the impact was closer to 20 μm [18]. These figures compare favourably with the heights measured by Inada et al. [10] for a 2°C subcooled droplet impacting on a 420°C copper surface with a similar impact Weber number. Encouragingly, both the experimental and simulated data show that the height of the vapour layer prior to recollection and rebound from the surface was highly oscillatory.

The maximum local Knudsen number calculated during this impact was 0.04. This level of the local Knudsen number implies that the effective slip velocity at either the liquid–vapour interface or solid–vapour interface was approximately 20% of the average vapour velocity within the vapour layer at the measuring location. Thus, the effect of the kinetic theory momentum treatment used in the vapour layer model was significant during this impact.

The gold impact material used in the experiments was highly polished. According to Boundy [19], such a surface would typically have a roughness amplitude of approximately 25 nm, which is considerably less than the minimum vapour layer height experienced during the impact. Also, a Rayleigh–Taylor instability analysis conducted on the lower surface of the droplet indicated that undulations of the liquid surface during the impact would be insignificant [18]. For these reasons it is expected that no direct liquid–solid contact occurred during the Wachters and Westerling $We = 15$ impact.

2.2. The Wachters and Westerling $We = 74$ impact

The second droplet dynamics experiment presented in Wachters and Westerling [2] was performed using identical conditions to the first, except that the impact velocity of the droplet was increased to 1.41 m/s, giving a Weber number for the impact of 74. Fig. 3(a) shows the photographs by Wachters and Westerling of this impact, and Fig. 3(b) the BOUNCE simulation.

A comparison of the experimental and computational images shows that the initial stages of the $We = 74$ impact are predicted well by BOUNCE. From 0.4 to 1.3 ms, the experimental photographs show a jet of liquid spreading across the surface of the solid, emanating from the droplet solid impact region. The BOUNCE simulation predicts this behaviour accurately, in particular the rounding of the advancing edge of the jet by surface tension forces, and the slight upward movement of the jet evident between 0.9 and 1.4 ms.

At 2.2 ms, the BOUNCE simulation predicts that the leading edge of the liquid jet separates from the main bulk of the droplet, forming a toroid of liquid with a small cross-sectional diameter. The resolution of the experimental images precludes validation of such separation, so it is not possible to ascertain whether this behaviour is physical. However, experimental images do show that the height of the droplet around the circumference is not uniform. The geometry of the top surface of the main droplet volume is predicted accurately at this time.

From approximately 3–6 ms, the BOUNCE simulations show the droplet separating into several more toroids of liquid, which spread radially outward over the computational domain. During the same period the experimental images show the liquid mass oscillating in a comparatively more random, asymmetrical manner. The difference between the two results can be attributed to the coordinate system in which the computations are performed.

The asymmetrical oscillations shown during the experimental impact involve a significant amount of surface, internal kinetic and external kinetic energy. These oscillations cannot be represented using the two-dimensional coordinate system employed by BOUNCE, as simulated fluid variables can only vary in the radial and axial directions. Instead, during the simulated impact, toroids of fluid are ejected at the circumference of the droplet, and these toroids, which are not physically realistic entities, expand until a sufficient amount of internal and external kinetic energy of the droplet has been converted to potential surface energy.

Beyond 6 ms, the correlation between the experimental and computational impacts continues to deteriorate. The experimental droplet recollects during this period, forming a small diameter elongated droplet and a much smaller ejected droplet by the last frame of the experimental figure. The simulated droplet on the other hand remains as several separate masses of fluid, the outer toroids of fluid not being given sufficient time to return to the centre of the computational domain and

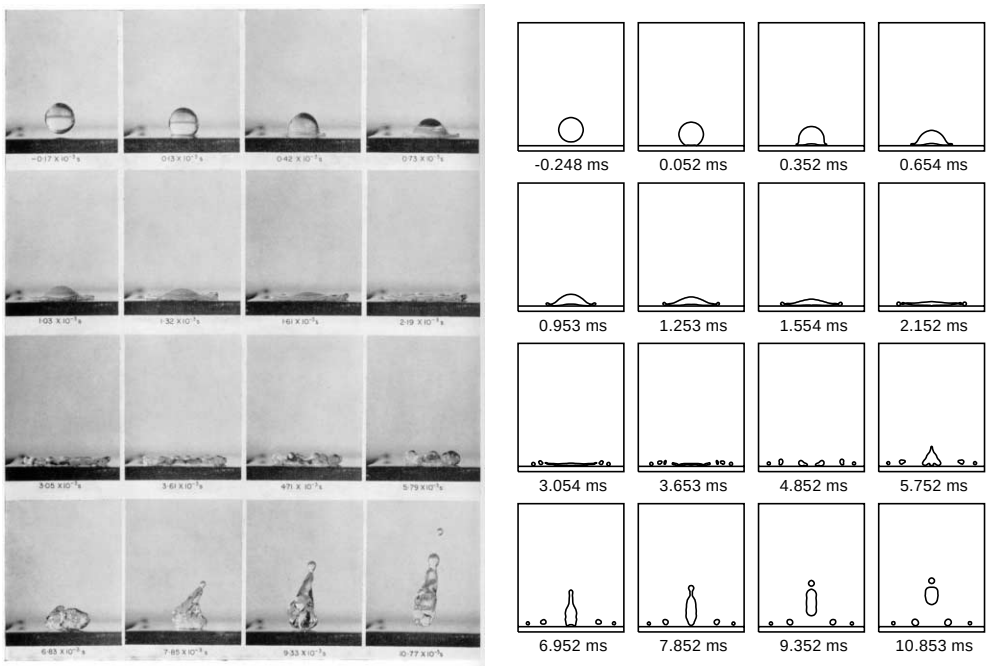

(a) experiment **(b)** simulation

Fig. 3. The $We = 74$ impact performed by Wachters and Westerling. Frame (a) shows the experimental photographs (taken from [2]), while frame (b) shows the simulation results. The initial diameter of the droplet was 2.3 mm.

reform into one mass. It is clear that the BOUNCE simulation is only applicable in the initial impact and spreading phase of this impingement.

The Wachters and Westerling impact simulations presented here, along with higher velocity simulations presented in Harvie [18], demonstrate that at Weber numbers of less than 30, BOUNCE is able to predict the impact, spreading and rebound phases of droplet impact behaviour. At Weber numbers between 30 and 80, BOUNCE predicts the important impact and spreading phases, but fails to reproduce the disintegration and subsequent re-formation of such impacts because of the two-dimensional coordinate system that is employed. At Weber numbers higher than 80, BOUNCE is only able to predict the initial impact behaviour of the main fluid body of each droplet.

2.3. The Groendes and Mesler impact

In this section we again compare the hydrodynamic behaviour of a simulated and experimental impact, but also compare the solid surface temperatures measured during the impact against the same temperatures calculated by BOUNCE. This provides a more direct validation of the viscous vapour layer model, and the thermodynamic ability of BOUNCE to simulate a saturated film boiling impingement. The experiment used to make this comparison is taken from the study by Groendes and Mesler [5], already discussed in Section 1.

Fig. 4(a) shows photographs of the actual Groendes and Mesler droplet impact, while Fig. 4(b) shows the equivalent BOUNCE simulation. This impact was performed on a low thermal diffusivity quartz impact material, initially heated to 462°C. The Weber number was 68.

The hydrodynamic behaviour of the Groendes and Mesler impact, and the simulation of the impact, share similarities with the Wachters and Westerling $We = 74$ example considered in the previous section. The first five frames of both the experimental and simulated images show the droplet impacting with, and spreading over, the solid surface. The correlation between the images is good here, with the BOUNCE simulation accurately predicting the behaviour of the jet formed at the intersection between the liquid and solid materials. The BOUNCE simulation shows that at approximately 5.3 ms, the centre of the underside of the droplet moves towards the solid for a second time during the impingement. This initiates a secondary wave along the underside of the droplet, which moves from the axis of the computational region radially outwards.

By 8.3 ms, the droplet has almost reached the maximum radius of the impact, and the simulation shows that the thickness of the liquid sheet is small, especially

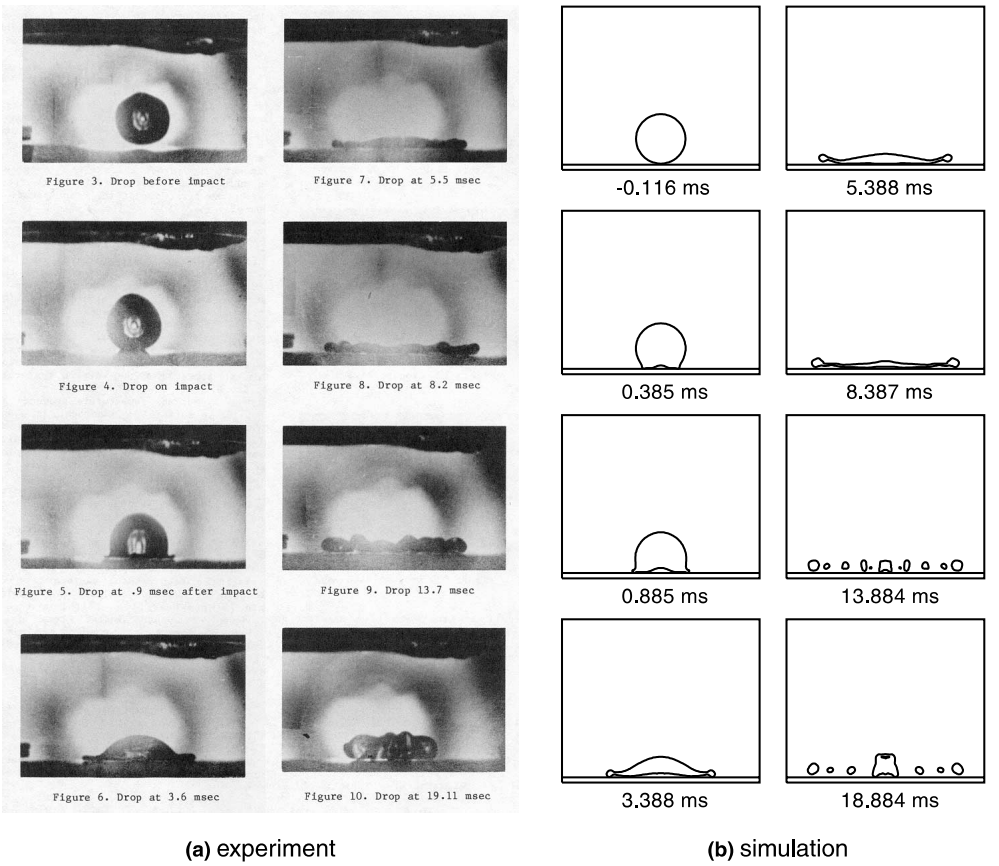

Fig. 4. The Groendes and Mesler water droplet impact. Frame (a) shows the experimental photographs (taken from [5]), while frame (b) shows the simulation results. The initial diameter of the droplet was 4.7 mm.

near the perimeter of the droplet. The photographic image at the same time supports the simulated image qualitatively, although the resolution of the experimental image is not high enough to determine the geometry of the droplet within the outer perimeter region, and the experimental droplet is starting to show small asymmetrical variations in thickness.

From 13 ms and onwards, the Groendes and Mesler droplet behaves in a similar fashion to the $We = 74$ Wachters and Westerling impact, having begun to oscillate in an asymmetrical manner. The images from the simulated impact show that the simulated droplet has broken into a large number of non-physical concentric toroids, which have spread a large distance from the centre of the impact region. This behaviour, as was previously discussed, is due to the two-dimensional coordinate system used by BOUNCE.

Although not shown in Fig. 4, at times beyond 20 ms, the correlation between the experimental and simulated impact continues to deteriorate [18]. By approximately 30 ms, the experimental results show that the actual droplet reforms, and begins to slowly move away from the solid surface. However, only a proportion of the simulated droplet reforms by 30 ms, the remainder residing in the vicinity of the solid in the form of several large diameter toroids.

Fig. 5 shows the solid surface temperatures measured during the Groendes and Mesler impact, and Fig. 6(a) the vapour layer interface temperatures calculated during simulation of the same impact.

The correlation between the solid surface temperatures shown in Figs. 5 and 6(a) over the first 15 ms of the impact is good. The BOUNCE simulation predicts the form and magnitude of the initial temperature decrease accurately. This decrease corresponds to the underside of the droplet first interacting with the solid surface.

At approximately 5.5 ms, the solid surface temperatures in both the computational and experimental results again decrease. The temperature drop shown in the experimental results confirms the prediction that the underside of the droplet moves towards the solid surface twice during the initial impact and spreading of the droplet over the solid surface. The form of the temperature decrease in the experimental results is less

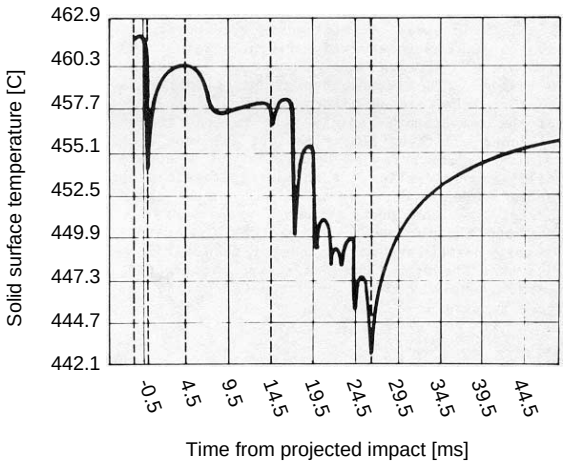

Fig. 5. The solid surface temperature measured beneath the Groendes and Mesler subcooled water droplet impact (taken from [5]).

severe than the decrease shown in the computational results, probably because either the experimental temperature represents an average over the large surface measurement region beneath the droplet, or the axis of the droplet is not positioned directly over the area of the thermocouple. Note that the computational temperature represents the temperature at the centreline of the droplet.

At approximately 15 ms from the initial impact, the experimental and simulated solid surface temperatures both begin a series of fairly rapid oscillations, as the centre of the underside of the droplet oscillates towards and away from the solid surface [18]. Despite the droplets differing in geometrical form at these times, the solid surface temperatures are reasonably well predicted. The minimum temperature of the solid measured from the experiment was approximately 443°C during this period, while the simulation predicted approximately 444°C.

The experimental results of Fig. 5 show that the centre of the underside of the droplet leaves the vicinity of the solid surface at approximately 27 ms, while the simulated impact predicts the same behaviour at approximately 33 ms. It is interesting that the non-physical formation of separate toroids of fluid in the simulated results did not substantially affect the behaviour of the solid surface temperature at the centre of the computational domain.

The correlation between the experimental and computational solid surface temperatures discussed above suggests that BOUNCE is correctly calculating the energy fluxes at the solid–vapour and liquid–vapour interfaces during this saturated film boiling impact.

Fig. 6(a) also shows vapour layer centreline temperatures at both the liquid–vapour and solid–vapour interfaces, as well as the liquid temperature at the same location, calculated during the Groendes and Mesler impact simulation. The temperature of the liquid and vapour at the liquid–vapour interface remains within a few degrees of the saturation value at all times. The several peaks in these variables coincide with the droplet approaching the solid surface. The temperature discontinuities at the liquid–vapour and solid–vapour interfaces are small in comparison with the temperature difference between the liquid and solid phases. Consequently, they have only a minor effect on the calculated heat transfer rates across the vapour layer during this impact.

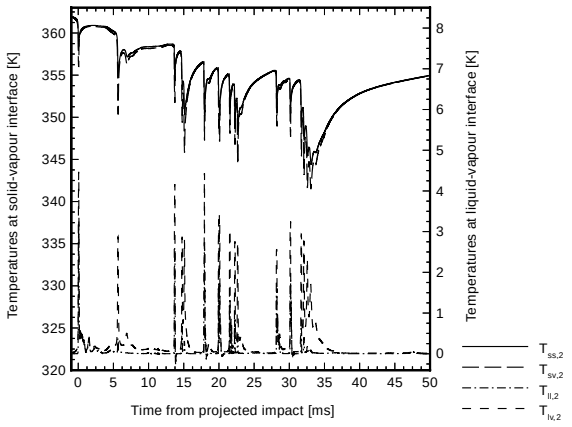

(a) vapour layer temperatures

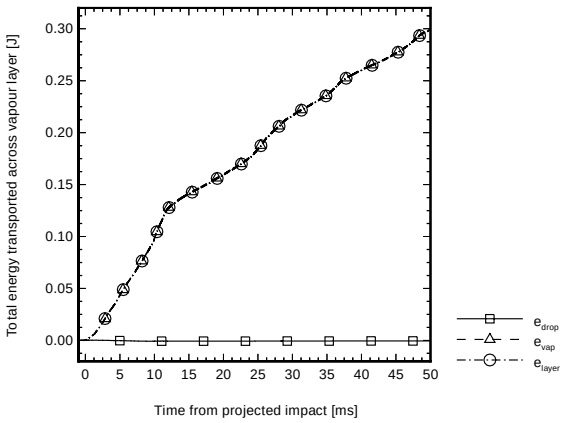

(b) vapour layer energy transfer

Fig. 6. Vapour layer interface temperatures (a) and total energy transported (b) during the simulated Groendes and Mesler impact. The temperatures are located below the axis of the droplet, and are measured relative to the saturation temperature of water at atmospheric pressure. In frame (b) the total energy conducted into the body of the droplet during the impact is represented by e_{drop}, the total energy consumed by vaporisation of liquid by e_{vap}, and the total energy transferred across the vapour layer by e_{layer}.

Finally, Fig. 6(b) shows itemised total energy transfer amounts occurring during the Groendes and Mesler impact. As indicated, the energy that is conducted into the droplet fluid during the impact is negligible, the majority of energy crossing the vapour layer going into vaporising liquid. The amount of energy extracted from the solid continues to rise at times after 50 ms from impact, as in the simulation, a toroid of fluid remains within the vicinity of the solid long after the main body of fluid has departed.

The energy lost by the solid at the actual time of droplet rebound, approximately 40 ms, is approximately 0.24 J, which represents the latent heat of vaporisation of only 0.18% of the droplet volume. Such a low proportion of droplet volume vaporised is consistent with the saturated impact measurements of Wachters and Westerling [2], and indicates the low efficiency, in terms of heat extracted from the solid surface, of saturated film boiling droplet impacts.

3. Subcooled film boiling droplet impacts

3.1. Hydrodynamic behaviour

To validate the ability of BOUNCE to reproduce the hydrodynamic behaviour of subcooled impacts, a simulation was performed of a low gravity *n*-heptane impact presented in Qiao and Chandra [7]. Fig. 7(c) shows the experimental impact, while Fig. 7(d) shows the simulation. In both cases, the temperature of the solid surface was initially 210°C, the diameter of the droplet was 1.5 mm and the Weber number for the impact was 32. The fluid was initially at room temperature, giving a droplet subcooling of approximately 75 K. The computations were performed using 60×210 square mesh cells over a computational domain of 0–1.8 mm radially, and −0.06–6.24 mm axially. The 16 ms of simulation required approximately 12,200 iterations, giving an average timestep of approximately 1.3 μs.

A comparison of the experimental and simulated images indicates that BOUNCE simulates the hydrodynamics of the low gravity *n*-heptane impact well. Until approximately 3 ms, the computational and experimental images show that BOUNCE predicts the formation and expansion of a jet at the interface between the solid and liquid phases, and replicates the rounding of this jet by surface tension forces. The slight upward movement of the lower surface of the jet at times beyond 1 ms is also predicted accurately by the code.

While the computational and experimental images generally correlate well during the impact and spreading period, the correlation between the first experimental image and the corresponding computational image is less satisfactory. The label adjacent to the first experimental image indicates that the image was taken 0.2 ms after the droplet impacted the solid surface. During this 0.2 ms, the top of the droplet would have travelled approximately 0.16 mm towards the solid surface, or roughly one tenth of the initial height of the droplet. Examination of the experimental photograph in Fig. 7(c) shows that at the indicated 0.2 ms, the top of the droplet has advanced further than one tenth of the initial height of the droplet towards the solid surface. This suggests that the first experimental image actually represents the droplet position at a time significantly after 0.2 ms from initial impact, rather than as indicated in the figure.

At 4 ms, the experimental images show that only a thin layer of fluid exists at the axis of the droplet, and the majority of the fluid is contained within a large flat toroid. BOUNCE predicts this behaviour accurately, in particular the downward 'crimping' of the central thin sheet at the inner radius of the toroid.

Over the next few milliseconds, the droplet recollects and rebounds from the surface. At 6.6 ms, the experimental images show that the droplet has formed a rough 'witch's hat' shape, and by 13.6 ms, the droplet is in the form of a triple dumb-bell shape and has left the surface. BOUNCE predicts this behaviour well, in particular the rounding of the top of the droplet at 6.6 ms by surface tension forces, and the unusual form shown in the last experimental frame.

3.2. Thermodynamic behaviour

3.2.1. Vapour layer interface temperatures

To validate the ability of BOUNCE to predict the thermodynamic behaviour of subcooled droplet impacts, the surface temperatures measured during an actual impact are compared against those calculated during a simulated impact. The experimental impact is again taken from Qiao and Chandra [7]. The experimental conditions are the same as those used in the impact shown in Fig. 7(c), except that the initial surface temperature has been increased to 300°C.

The solid line in Fig. 8 shows the centreline vapour layer interface temperatures calculated by BOUNCE during the 300°C impact. During the first 2 ms of the impact, this temperature decreases rapidly as the droplet impacts and deforms across the surface of the solid. Such a rapid temperature decrease is due to the small central vapour layer height existing during this period, which allows a large heat transfer rate from the solid within the central region.

After 2 ms, the vapour layer height at the centre of the impact region increases as the droplet spreads over the surface of the solid. This reduces the heat transfer rate from the central solid region, in turn causing the central solid surface temperature to stabilise. By the end of the first expansion period, the central surface temperature is approximately 5 K below the initial temperature.

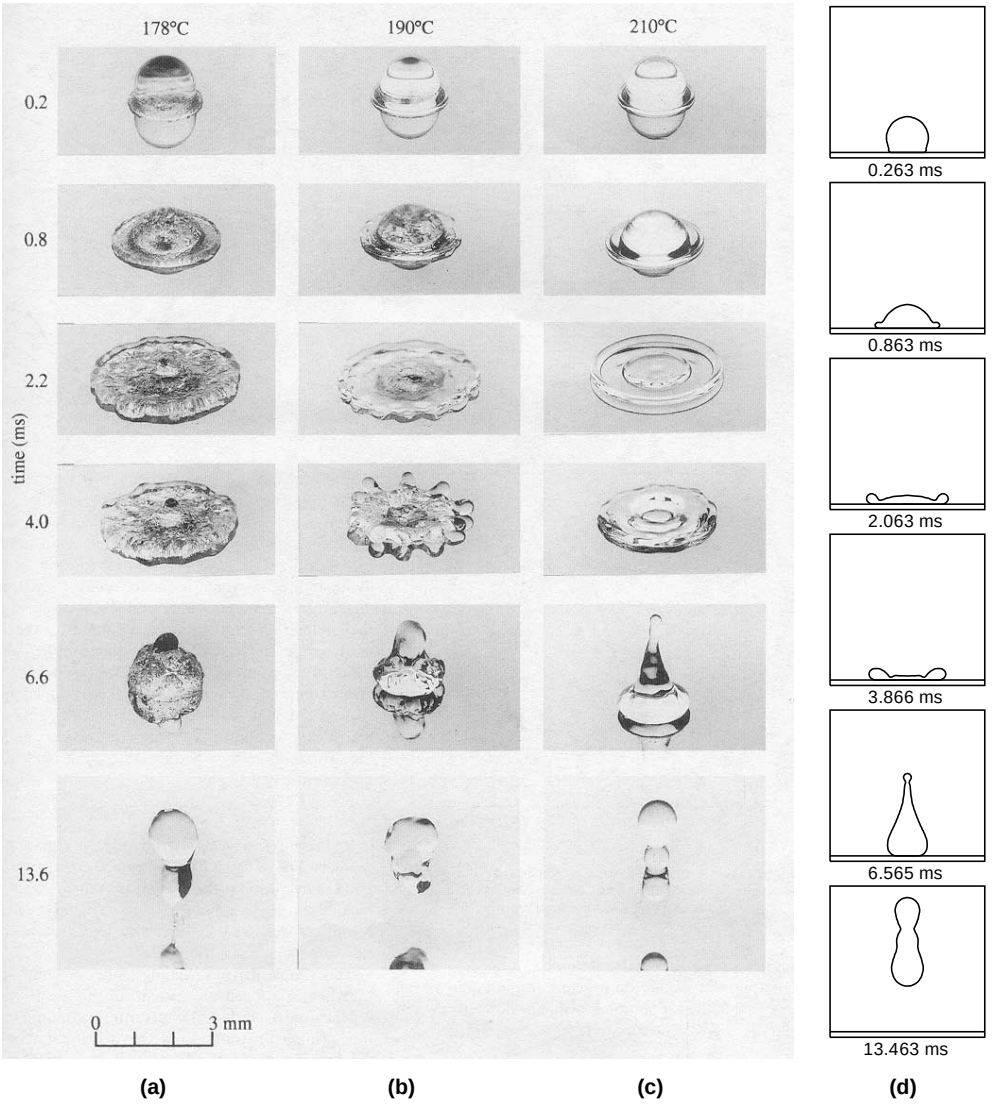

Fig. 7. Three low gravity experimental *n*-heptane impacts conducted at different initial solid temperatures (a)–(c), and one simulation (d). Case (a) refers to the 178°C impact, case (b) to the 190°C impact and case (c) to the 210°C impact (taken from Qiao and Chandra [7]). Case (d) is a simulation of the 210°C case (c) impact. The initial diameter of these droplets was 1.5 mm.

After 5 ms, the droplet begins to recollect and rebound from the surface. As this process occurs, the centre of the droplet is again forced towards the solid, and as a result, the solid temperature at the axis of the droplet decreases sharply. In the period between 5 and 9 ms, the central solid surface temperature drops a further 11 K. After 9 ms, the droplet leaves the vicinity of the solid surface, and the surface temperature at the axis of the droplet gradually increases as heat diffuses from within the body of the solid towards the surface.

The centreline vapour temperature at the solid–vapour interface is also shown in Fig. 8. As shown, the temperature discontinuity occurring at the solid–vapour interface is most significant when the heat transfer rate from the solid is high. However, as for the saturated impacts discussed previously in this study, the magnitude of the temperature discontinuity across the solid–vapour interface is at all times an order of magnitude smaller than the temperature difference across the vapour layer, so consequently, the effect of this discontinuity on the heat transfer calculation is not significant.

Fig. 8 also shows the centreline temperatures at the liquid–vapour interface of the droplet. After the droplet impacts the solid, the temperature of the liquid quickly increases from the initial ambient value, as heat is conducted into the body of the droplet. At approximately

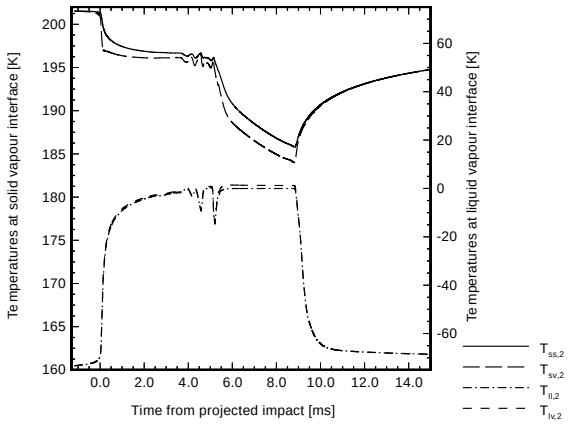

Fig. 8. Temperatures at the liquid–vapour and solid–vapour interfaces calculated during the low gravity Qian and Chandra impact. Temperatures shown in this figure are measured relative to the saturation temperature of *n*-heptane at atmospheric pressure.

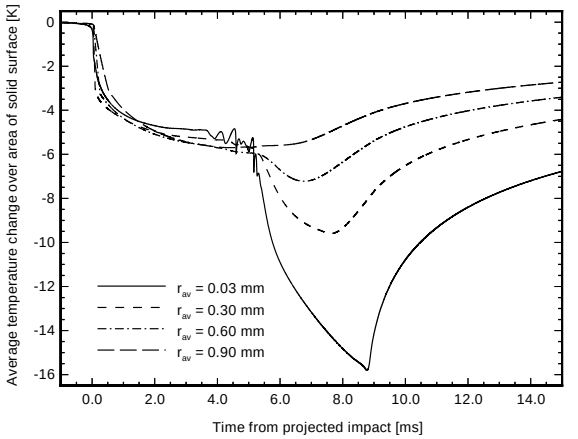

Fig. 9. The solid surface temperature drop under a low gravity *n*-heptane impact. The four curves shown represent temperatures averaged over a circle of radius r_{av} on the surface of the solid, concentric with the axis of the droplet.

9 ms, the impact process is completed and the droplet begins to move away from the solid. From this point onwards the temperature of the liquid decreases, asymptotically approaching the ambient temperature of the surroundings. The temperature discontinuity occurring across the liquid–vapour interface is at all times small in comparison with the temperature difference across the vapour layer.

The maximum central solid surface temperature decrease calculated during the simulated Qiao and Chandra impact was approximately 15.7 K. This value does not compare well with the experimental results presented in Qiao and Chandra [7], where the maximum temperature decrease found during actual impacts on a 300°C surface was approximately 6.9 K. The poor correlation probably results from a difference in temperature measurement methods used in the experimental and simulated impacts.

The temperature measurements were made in the experimental impacts using a flush mounted commercially available thermocouple. However, it is not entirely clear over what area beneath the droplet the thermocouple measured the solid temperature, or how precisely the centre of the droplet impacted the centre of the region in which the solid temperature was measured.

To allow comparison between the simulated and experimental results, four temperature drop curves are shown in Fig. 9. Each curve represents the average solid temperature within a circle on the surface of the solid, of radius r_{av}, and concentric with the axis of the droplet. Thus, each curve shown in Fig. 9 is calculated using an average temperature over a finite area of the solid surface.

The first curve shown in Fig. 9 was calculated using a circle of radius $r_{av} = 0.03$ mm. This curve approximately represents the solid surface temperature drop at the axis of the droplet, and uses the same data as used for the solid surface temperature curve of Fig. 8. The remaining three curves were calculated using circles having radii of 0.3, 0.6 and 0.9. The initial radius of the droplet in this simulation was 0.75 mm.

The results of Fig. 9 show that as the area over which the solid surface temperature is measured is increased, the magnitude of the temperature drop during the recollection and rebound phase of the impact decreases. As discussed above, during the recollection phase of the impact, the centre of the droplet is forced towards the solid, which increases heat transfer rates within this region. Consequently, the solid surface temperature at the axis of the droplet decreases significantly during this phase, while the solid surface temperatures in regions away from the axis tend to increase slightly. As a result, the larger the area over which the solid surface temperature is measured, the lesser the impact the central temperature drop has on the average value, and the smaller the average temperature drop is during the recollection phase of the droplet impact. Interestingly, the solid surface temperature drop during the initial impact and expansion phase of the simulation is only weakly affected by the area over which it is averaged.

Comparing the experimental maximum solid temperature drop of 6.9 K and the simulated results shown in Fig. 9, the best correlation between the two occurs when the simulated temperature is averaged over a circle of radius $r_{av} = 0.6$ mm. This appears to be a physically credible dimension for the thermocouple used in the Qiao and Chandra experiments, and consequently, the difference in solid surface temperature drops between the experimental and computational impacts can be

satisfactorily explained by the effect of area averaging due to the finite thermocouple dimensions.

3.2.2. Vapour layer composition and thermal energy transfer

The centreline vapour layer air volume fraction during the same 300°C *n*-heptane impact is shown in Fig. 10(a). During the initial expansion stage of the impact, the air volume fraction decreases rapidly as liquid vaporises at the underside of the droplet and the height of the vapour layer decreases. At around 5 ms from initial impact, the air volume fraction displays some large oscillations, a result of the oscillatory and small height of the vapour layer during this short period. When the impact process has been completed and the droplet begins to move away from the surface, the air volume fraction rapidly increases again as vapour mixture from the surrounding atmosphere is drawn into the region beneath the recoiling droplet.

Fig. 10(b) shows the total energy transported across the vapour layer during the same 300°C low gravity *n*-heptane impact. The total amount of energy lost by the solid during this impact is approximately 0.019 J, the majority of this having been used to heat the liquid contained within the droplet. The total droplet volume vaporised during this impact was only 0.05% of the initial volume. The maximum calculated heat transfer rate from the solid at the axis of the droplet during this impact was approximately 2.0×10^6 W/m^2.

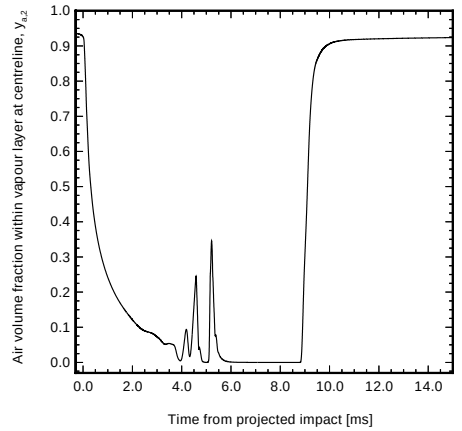

(a) vapour layer composition

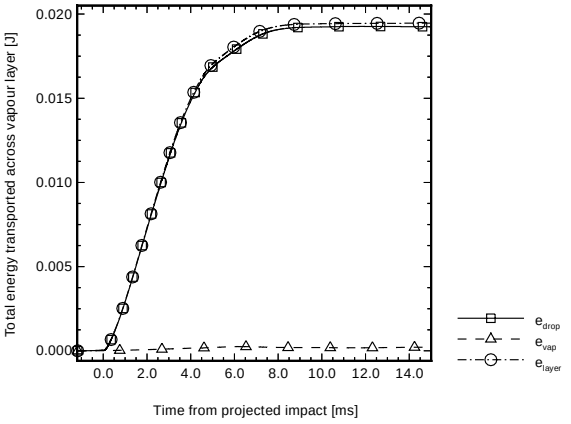

(b) vapour layer energy transfer

Fig. 10. Vapour layer composition (a) and total energy transported (b) during the simulated low gravity Qiao and Chandra impact with the initial solid temperature of 300°C. In case (b), the total energy conducted into the body of the droplet during the impact is represented by e_{drop}, the total energy consumed by vaporisation of liquid by e_{vap}, and the total energy transported across the vapour layer by e_{layer}.

3.3. Saturated and subcooled impacts

It is interesting to compare the behaviour of the saturated droplet impacts presented in Section 2 with the subcooled impact presented here. After the initial impact, the underside of a saturated droplet moves sharply upward, creating a 'dome' of vapour under the axis of the droplet. In the subcooled impact however, the underside of the droplet remains close to the solid surface after the initial impact, so that the height of the vapour layer appears to be smaller and more uniform than for the saturated impacts. The difference in behaviour can be explained in terms of an energy balance at the lower liquid–vapour interface of the droplet.

When a saturated droplet moves towards a solid surface, pressures generated in excess of atmospheric allow the temperature of the lower surface of the droplet to increase above the ambient saturation temperature. After the initial impact however, the vapour layer pressure decreases, as the pressure required to sustain the lower droplet surface above the solid is less than was required to decelerate the droplet during the impact. As the pressure decreases, the temperature of the lower surface of the droplet must also decrease. To facilitate this energy loss, the liquid is vaporised, and the lower surface of the droplet is forced away from the solid, creating the visible 'dome' of vapour beneath the droplet.

When a subcooled droplet moves towards a solid surface, the same processes occur until the vapour layer pressure which decelerates the droplet starts to decrease. At this stage, during a subcooled impact, heat can be conducted into the body of the liquid to decrease the lower droplet surface temperature, rather than being used to vaporise liquid. Consequently, the lower surface of a subcooled droplet is able to stay closer to the solid, and the vapour layer height appears to be smaller and less oscillatory with time.

Note that it is for these same reasons that the liquid and solid interface temperatures do not show the same degree of oscillation under a subcooled impact than are displayed during a saturated impact.

3.4. Droplet impact boiling regimes

The continuous curve of Fig. 11 shows the relationship between the maximum solid surface temperature decrease during experimental *n*-heptane impacts, and the initial temperature of the solid. The curve has been reproduced from the study by Qiao and Chandra [7], and is applicable to both low gravity and normal gravity impacts conducted with an initial Weber number of 32.

Fig. 11 shows that the maximum solid temperature drop during the experimental impacts peaks within an initial solid temperature range of 160–200°C. In the initial temperature range of 200–230°C, the temperature drop decreases sharply with increasing initial temperature, but this decrease gradually relaxes as the initial solid temperature approaches 300°C.

Fig. 11 also shows solid surface temperature drops calculated by BOUNCE for low gravity *n*-heptane simulations performed with initial solid surface temperatures of 300°C, 250°C, 200°C, and 150°C. Each temperature drop was calculated using surface temperatures averaged over a circle of radius $r_{av} = 0.6$ mm, and the remaining aspects of each computation were the same as used for the low gravity *n*-heptane impact shown in Fig. 7(d).

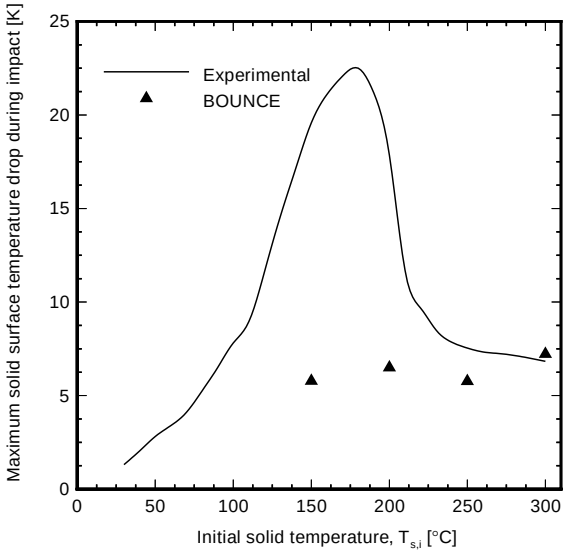

Fig. 11. The maximum solid surface temperature drop occurring during *n*-heptane impacts as a function of the initial temperature of the solid. The continuous curve is taken directly from Qiao and Chandra [7], and is valid for both low gravity and normal gravity impacts with an initial Weber number of 32. The points indicate results predicted by BOUNCE.

A comparison between the experimental and simulated results of Fig. 11 shows that at the initial surface temperature of either 250°C or 300°C, the correlation between the simulated and experimental results is reasonable, but at initial solid temperatures of 200°C and below, the correlation is poor. Interpolating the simulated data between 200°C and 250°C suggests that the initial solid temperature of 230°C approximately marks the temperature boundary between impacts that BOUNCE simulates thermodynamically, and those it does not.

That BOUNCE simulates the temperature drop occurring during the 300°C impact is not remarkable. The radius over which the simulated temperature drop was averaged was determined to correlate the experimental and computational data at this temperature. However, that BOUNCE reasonably predicts the solid surface temperature drop down to an initial solid temperature of approximately 230°C suggests that impacts occurring above this temperature are film boiling impacts, as BOUNCE is a purely film boiling code. At temperatures below 230°C BOUNCE is not able to predict the thermodynamic behaviour of the droplet, because impacts occurring below this initial solid temperature are either transition or nucleate boiling impacts.

As well as showing the impacts that were examined in Section 3.1, Fig. 7 also shows experimental impacts that were conducted with initial surface temperatures below 200°C. It is clear from these images that in these cases vapour bubbles are forming at the liquid–solid interface, and nucleate boiling is occurring. During nucleate boiling impacts the heat transfer rates experienced at the surface of the solid are far higher than the heat transfer rates experienced during film boiling impacts, because prolonged contact between the liquid and solid phases occurs. Consequently, the experimental temperature drops measured below 200°C are much higher than those predicted by the film boiling BOUNCE code.

As impacts occurring over the initial solid temperature of 230°C are film boiling impacts, and impacts occurring below the initial solid temperature of 200°C are nucleate boiling impacts, we can assume that impacts occurring in the temperature range of 200°C to 230°C are transition boiling impacts. During transition boiling impacts, direct solid–liquid contact occurs, but only for a short duration.

The simulation shown in Fig. 7(d) was performed using an initial solid temperature of 210°C, so as a consequence, this impact was actually a transition boiling impact. Thus, while BOUNCE is not able to predict the thermodynamics of such impacts, it is able to simulate the hydrodynamics of transition boiling impacts. BOUNCE is predicting the hydrodynamic behaviour of transition boiling impacts because the duration of

contact between the solid and liquid phases is much shorter than the timescale of gross droplet deformation. Thus, the short contacts do not affect the hydrodynamics of the droplet. BOUNCE is not predicting the thermodynamics of transition boiling impacts because the amount of energy transferred between the solid and liquid phases when contact occurs is large, even if as in this case, the duration of each contact is small.

3.5. Vapour layer destabilisation

BOUNCE is a film boiling code, and as such, no direct contact between the solid and liquid phases is modelled. Consequently, it is not surprising that BOUNCE is not able to model the thermodynamics of transition boiling impacts, or the thermodynamics and hydrodynamics of nucleate boiling impacts.

Determining possible reasons why BOUNCE does not predict the occurrence of solid–liquid contact during these lower temperature impacts is interesting however, for it gives us insight into possible mechanisms for actual impact vapour layer collapse, and also suggests possible development directions for BOUNCE and other two phase heat transfer codes.

With these objectives in mind, three assumptions that were used in the development of the vapour layer code are now examined to determine the relevance each has on vapour layer destabilisation.

3.5.1. Surface roughness or contamination

In the development of the vapour layer algorithm, it was assumed that the surface of the solid was perfectly smooth. If however, the impact surface has undulations which have sizes comparable with the thickness of the vapour layer, then solid spikes may protrude into the liquid phase, promoting locally high heat transfer rates, and thus invalidating calculated vaporisation velocities.

A surface which has been finely honed and polished, such as the surface used in the Qiao and Chandra [7] experiments, typically has a surface roughness value of $R_a \approx 25$ nm [19]. This measurement represents an average roughness amplitude, so the amplitude of the maximum undulations on such a surface may be as high as 0.1 μm [18].

A BOUNCE *n*-heptane impact simulation was performed using an initial solid surface temperature of 200°C, this being a solid temperature which is expected to cause vapour layer destabilisation. All other aspects of the simulation were the same as used for the impact shown in Fig. 7(d).

The minimum vapour layer height during the simulated 200°C impact was approximately 0.7 μm, and this minimum occurred during the initial stages of the impact. Although this height is an order of magnitude less than the height experienced during the saturated droplet impacts of Section 2, the undulations in the impact surface discussed above are not of this magnitude, so it is unlikely that 'spikes' of solid are protruding through the height of the vapour layer and contacting the liquid phase.

However, it is possible that dust or other foreign particles residing on the impact surface could traverse the 0.7 μm minimum vapour layer height. The experimentalists took many precautions to preclude the presence of foreign particles from the impact surface, however, it is suspected that eliminating sub-micron particles from the impact surface may be difficult. Consequently, no definite conclusions as to the effect of possible surface contaminations on vapour layer destabilisation can be drawn, except that it is recognised that their presence may aid vapour layer collapse.

3.5.2. Vapour layer molecular slip flow

The maximum Knudsen numbers predicted by BOUNCE beneath four low gravity *n*-heptane impacts are shown in Fig. 12. The Knudsen number is here defined as the ratio of the average molecular free path of the vapour mixture within the vapour layer to the height of the vapour layer. Each curve uses a different initial solid surface temperature, varying from 300°C down to 150°C. All other aspects of these computations are as used in the simulation shown in Fig. 7(d).

Fig. 12 shows that the maximum calculated Knudsen number within the vapour layer during the initial stages of each impact increases as the temperature of the solid surface decreases. At the lowest possible initial solid temperature before vapour layer collapse occurs, that is approximately 230°C, the maximum initial Knudsen number would be approximately 0.05.

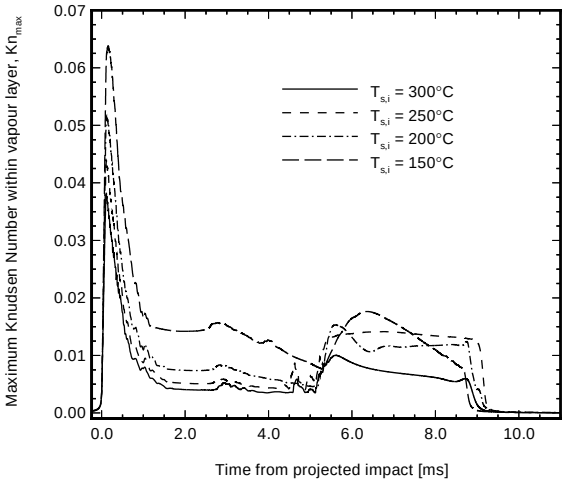

Fig. 12. The maximum Knudsen numbers beneath four simulated low gravity *n*-heptane impacts as a function of time.

The Knudsen numbers shown in Fig. 12 are determined using a two-dimensional coordinate system, and as such, represent the maximum of the average Knudsen numbers evaluated at each radial location. In reality however, the underside of a droplet may show small variations in vapour layer height as one rotates around the axis of the droplet. Thus, the actual maximum Knudsen numbers within the layer may be larger than those shown.

Also, the surface roughness discussion of the previous section indicated that at the limit of applicability of the BOUNCE code, surface undulations may be only an order of magnitude smaller than the calculated minimum vapour layer heights. Thus, the presence of surface undulations may also cause the calculated maximum Knudsen numbers to be underpredicted by BOUNCE.

The assumption utilised in the formulation of the vapour layer model was that the fluid flow beneath the droplet was in the molecular slip regime [1]. This means that the continuum fluid assumption is used within the body of the vapour layer, but that a molecular slip treatment is included at the interfaces of the vapour layer. It has been estimated that this regime is valid below a Knudsen number of 0.1, however, this number represents an order of magnitude limit rather than a precise figure [20].

Therefore, as the maximum Knudsen number within the vapour layer during the 230°C *n*-heptane impacts is at least 0.05, and as the slip molecular flow regime is valid only below a Knudsen number of the order of 0.1, a reason that the BOUNCE results are not applicable below 230°C may be that the continuum fluid assumption used within the vapour layer is no longer valid in these impacts. It is interesting to note that the Knudsen number of 0.05 was never exceeded in the saturated water impact simulations considered in Section 2 of this study.

The experimental results presented by Knudsen [21, pp. 21–25] show that once a gas flow moves beyond the slip flow regime and into the free molecule flow regime, the effective viscosity of the gas may reduce substantially. In the present application this reduction in effective viscosity may lead to a reduction of pressure beneath the droplet, and a subsequent collapse of the vapour layer.

3.5.3. Rayleigh–Taylor instabilities

An assumption that was implicitly used in the formulation of the vapour layer model was that the lower surface of the droplet was smooth, in comparison with the height of the vapour layer. This assumption may not be valid however, when the height of the vapour layer is very small, and the lower surface of the droplet is being accelerated upward. Under such conditions, Rayleigh–Taylor instabilities may develop at the lower surface of the droplet [22], causing ripples to form at the liquid–vapour interface. These ripples may result in a direct contact between the solid and liquid.

A classical Rayleigh–Taylor analysis was performed to find the minimum acceleration that the lower surface of the droplet must experience before surface instabilities may grow [18]. For a typical *n*-heptane impact, this minimum was found to be 1.3×10^6 m/s^2. Calculations performed on the low gravity *n*-heptane impact of Fig. 7(d) conservatively showed that the maximum acceleration experienced by the underside of the droplet was less than 10^5 m/s^2 at all times. Thus, it may be concluded that Rayleigh–Taylor instabilities are not responsible for initiating vapour layer collapse.

The above discussion has highlighted the main assumptions used by BOUNCE that may become invalid when collapse of the *n*-heptane vapour layer is imminent. It was found that it is unlikely that solid surface roughness or liquid surface Rayleigh–Taylor instabilities are important factors when predicting such vapour layer collapse.

What did appear to be important in predicting such behaviour was the correct modelling of the gas flow regime within the vapour layer. In order to correctly predict vapour layer collapse and thus transition boiling impacts, a transition or rarefied gas molecular flow analysis within the vapour layer may be required. It has also been recognised that contamination of the impact surfaces in the examined *n*-heptane impacts may have promoted vapour layer collapse, another factor not considered in the BOUNCE simulations.

Note that the behaviour of a droplet once any direct contact between the solid and liquid phases has occurred is beyond the scope of this study. For discussion on this topic, refer to Qiao and Chandra [7].

3.6. Subcooled water impacts

While only subcooled *n*-heptane impacts have been presented in this study, the simulation of subcooled water impacts using the BOUNCE code has been previously attempted by Harvie [18]. Unfortunately, it was found that BOUNCE was unable to reproduce the thermodynamic behaviour of any of the available experimental subcooled water impacts.

It was shown by Harvie [18] that the reason BOUNCE is unable to predict any of the available significantly subcooled water droplet experiments is because for all cases available, vapour layer collapse appears to occur during the impact process. The primary assumption that invalidates the BOUNCE results when vapour layer collapse is imminent is the assumption of a molecular slip flow regime existing within the vapour layer. Note that the *n*-heptane molecule, which has the chemical form $CH_3(CH_2)_5CH_3$, has a larger molecular collision volume than the water molecule, and as a

consequence, at the same temperature and pressure, the molecular free path of *n*-heptane is much smaller than that of water. This results in substantially different Knudsen numbers occurring during similar *n*-heptane and water droplet impact simulations.

It was also recognised by Harvie [18] that surface contaminations, which are not modelled by BOUNCE, may also contribute to vapour layer destabilisation during subcooled water droplet impacts.

4. Conclusions

The BOUNCE film boiling impact code has been validated using a number of experimental droplet impact studies. The code is successful in predicting the hydrodynamic behaviour of the impact, spreading and rebound phases of film boiling impacts when the Weber number for the impingement is below 30. At Weber numbers between 30 and 80, BOUNCE is able to predict the impact and spreading phases of the process, but is unable to predict the complex rebound behaviour of the droplet. At Weber numbers above 80, BOUNCE predicts the initial impact behaviour of the main body of droplet fluid, but fails to reproduce the rapid disintegration that occurs in such high velocity impacts. Deficiencies displayed by BOUNCE in reproducing the hydrodynamical aspects of the higher velocity impacts are shown to be a result of the two dimensional coordinate system employed by the algorithm.

The thermodynamic validity of the BOUNCE code has been examined by comparing documented solid surface temperature measurements made during various experimental impacts against surface temperatures calculated during simulations of the same impacts. BOUNCE has reproduced the solid surface temperatures reasonably well below both saturated water droplets and subcooled *n*-heptane droplets, however, the thermodynamic simulation of significantly subcooled film boiling water droplets has not been validated because experimental results for such impacts do not appear to be presently available [18].

In order to determine the limit of applicability of the BOUNCE model, an examination of the conditions within the viscous vapour layer prior to vapour layer collapse has been conducted. It was found that assumptions used by BOUNCE regarding impact surface roughness and liquid surface instabilities are unlikely to affect droplet behaviour prior to vapour layer collapse. It was found to be more likely that the BOUNCE results are inapplicable just prior to vapour layer collapse because the flow regime within the vapour layer is no longer in the molecular slip regime, an assumption used in the development of the model. It is also recognised that surface contaminations, a factor not considered by the model, may also affect vapour layer stability.

References

[1] D.J.E. Harvie, D.F. Fletcher, A hydrodynamic and thermodynamic simulation of droplet impacts on hot surfaces, Part I: theoretical model, Int. J. Heat Mass Transfer 44 (2001) 2633–2642.
[2] L.H.J. Wachters, N.A.J. Westerling, The heat transfer from a hot wall to impinging water drops in the spheroidal state, Chem. Eng. Sci. 21 (1966) 1047–1056.
[3] B.S. Gottfried, C.J. Lee, K.J. Bell, The Leidenfrost phenomenon: film boiling of liquid droplets on a flat plate, Int. J. Heat Mass Transfer 9 (1966) 1167–1187.
[4] K.J. Baumeister, F.F. Simon, Leidenfrost temperature – its correlation for liquid metals, cryogens, hydrocarbons and water, Trans. ASME: J. Heat Transfer (1973) 166–173.
[5] V. Groendes, R. Mesler, Measurement of transient surface temperatures beneath Leidenfrost water drops, in: U. Grigull, E. Hahne, K. Stephan. J. Straub (Eds.), Heat Transfer 1982, Proceedings of the Seventh International Heat Transfer Conference, Munich, Federal Republic of Germany, 1982, pp. 131–136.
[6] S. Inada, Y. Miyasaka, K. Nichida, Transient heat transfer for a water drop impinging on a heated surface (1st report effects of drop subcooling on the liquid–solid state), Bull. JSME 28 (1985) 2675–2681.
[7] Y.M. Qiao, S. Chandra, Boiling of droplet on a hot surface in low gravity, Int. J. Heat and Mass Transfer 39 (1996) 1379–1393.
[8] S. Chandra, C.T. Avedisian, On the collision of a droplet with a solid surface, Proc. R. Soc. Lond. A 432 (1991) 13–41.
[9] J.C. Chen, K.K. Hsu, Heat transfer during liquid contact on superheated surfaces, J. Heat Transfer 117 (1995) 693–697.
[10] S. Inada, Y. Miyasaka, K. Sakamoto, K. Hojo, Liquid–solid contact state and fluctuation of the vapor film thickness of a drop impinging on a heated surface, J. Chem. Eng. Jpn. 21 (1988) 463–468.
[11] F.K. McGinnis III, J.P. Holman, Individual droplet heat-transfer rates for splattering on hot surfaces, Int. J. Heat and Mass Transfer 12 (1969) 95–108.
[12] J.P. Holman, P.E. Jenkins, F.G. Sullivan, Experiments on individual droplet heat transfer rates, Int. J. Heat and Mass Transfer 15 (1972) 1489–1495.
[13] C.O. Pedersen, An experimental study of the dynamic behavior and heat transfer characteristics of water droplets impinging upon a heated surface, Int. J. Heat and Mass Transfer 13 (1970) 369–381.
[14] M. Seki, H. Kawamura, K. Sanokawa, Transient temperature profile of a hot wall due to an impinging liquid droplet, Trans. ASME J. Heat Transfer 100 (1978) 167–169.
[15] K. Makino, I. Michiyoshi, Technical notes: the behavior of a water droplet on heated surfaces, Int. J. Heat and Mass Transfer 27 (1984) 781–791.
[16] T.Y. Xiong, M.C. Yuen, Evaporation of a liquid droplet on a hot plate, Int. J. Heat and Mass Transfer 34 (1991) 1881–1894.
[17] J.D. Bernardin, C.J. Stebbins, I. Mudawar, Mapping of impact and heat transfer regimes of water drops impinging on a polished surface, Int. J. Heat and Mass Transfer 40 (1997) 247–267.

[18] D.J.E. Harvie, A hydrodynamic and thermodynamic simulation of droplet impacts on hot surfaces. Ph.D. thesis, Department of Mechanical and Mechatronic Engineering, University of Sydney, NSW, Australia, 1999.
[19] A.W. Boundy, Engineering Drawing, third ed., McGraw-Hill, Sydney, 1986.
[20] W.M. Rohsenow, H. Choi, Heat, Mass, and Momentum Transfer, Prentice-Hall, Englewood Cliffs, NJ, 1961.
[21] M. Knudsen, Kinetic Theory of Gases, third ed., Methuen and Co., London, 1950.
[22] M. Pilch, C.A. Erdman, A.B. Reynolds, Acceleration induced fragmentation of liquid drops, Technical Report CR-2247, NUREG, 1981.